



## Abstract

Cross-shore transport of larvae, pollutants, and sediment between the surf zone and the inner shelf is important for coastal water quality and ecosystems. Rip currents are known to be a dominant pathway for exchange, but the effects of horizontal temperature and salinity gradients are not well understood. Airborne visible and infrared imagery performed on the California coast show warm and cool plumes driven by rip currents in the surf zone and extending onto the shelf, with temperature differences of approximately 1°C. The airborne imagery and modeled temperatures and tracers indicate that warm plumes exhibit more lateral spreading and transport material in a buoyant near-surface layer, whereas cool plumes move offshore in a subsurface layer. The average cross-shore extent of warm plumes at the surface is approximately one surfzone width larger than for cool plumes. Future work may explore the sensitivity of nearshore plumes to density patterns, wave forcing, and bathymetry.

## Plain Language Summary

Waves and currents in the coastal ocean move plankton, pollutants, nutrients, and sediment between the beach and deeper waters, impacting ecosystems and water quality. Rip currents, strong narrow seaward currents caused by breaking waves, provide a conduit for larvae to move offshore and also carry pollutants away from the beach. One common type of rip current formed in channels interrupting sandbars can sometimes be observed as a plume of brown sediment-laden water moving offshore. Previous studies of this rip-current type have assumed that the movement of material by these currents is not affected by differences in the water density (temperature and salinity) between shallower and deeper water. However, thermal (infrared) images taken from an aircraft on the coast of California show that the wave-breaking region near the beach is often significantly cooler or warmer than the ocean immediately offshore. Rip currents in these images and in numerical simulations appear either as warm plumes, which carry material further offshore and are concentrated at the water surface, or cool plumes, which move material offshore under the surface. The results show that differences in water temperature from the beach to deeper water impact how rip currents move material in the coastal ocean.

## 1 Introduction

Transport pathways of pollutants, nutrients, sediment, larvae, and heat in the transition from the shoreline to the shelf are important for coastal ecosystem health and water quality (Grant et al., 2005; Boehm et al., 2017). Bathymetric rip currents, strong seaward currents generated by wave breaking on channels and other alongshore-varying bathymetry in the surf zone (Bowen, 1969), are a dominant driver of cross-shore exchange in this region (Morgan et al., 2018). Signatures of rip-current circulation patterns can be observed extending onto the shelf, sometimes in the form of a turbid plume with elevated surface roughness (Smith & Largier, 1995; Haller et al., 2014) (Figure 1a). While the dynamics of bathymetric rip currents in the well-mixed surf zone are well understood and have been the subject of many observational and modeling studies (Dalrymple et al., 2011; Castelle et al., 2016), few studies have measured or assessed the importance of horizontal temperature and salinity variations as these currents evolve on the shelf.

Several field studies have observed that the surf zone may have a different temperature or salinity than water on the adjacent shelf, which is often stratified (Smith & Largier, 1995; Marmorino et al., 2013; Kastner et al., 2019; Hally-Rosendahl et al., 2014; Grimes, Feddersen, Giddings, & Pawlak, 2020). This may result in rip-current-driven nearshore plumes with a warm or cool temperature signature (Figure 1b,c). While temperature effects have not yet been investigated in persistent bathymetric rip current systems, the interaction of shelf stratification with stochastic surfzone eddy ejections, also known as

63 transient rip currents, has been investigated in modeling and observational studies (Hally-  
64 Rosendahl et al., 2014; Suanda & Feddersen, 2015; Grimes, Feddersen, Giddings, & Pawlak,  
65 2020; Grimes, Feddersen, & Kumar, 2020). Models have shown that, under stratified shelf  
66 conditions, transient rip currents eject eddies that move material several surfzone widths  
67 offshore in a subducted layer, thereby altering shelf stratification and circulation (Kumar  
68 & Feddersen, 2017a, 2017b, 2017c). However, the importance of horizontal density gra-  
69 dients between the surf zone and the inner shelf has not previously been investigated in  
70 detail using observations or models.

71 Bathymetric rip currents that form in channels at fixed locations (Dalrymple et al.,  
72 2011; Castelle et al., 2016) result in persistent plumes, differing from transient rip cur-  
73 rent processes that episodically eject material at changing locations. Fixed bathymet-  
74 ric rip current plumes may resemble other previously studied geophysical plume systems,  
75 including small river plumes (Cole & Hetland, 2016) when the surf zone is buoyant rela-  
76 tive to water on the shelf, or subduction at ocean fronts (Rudnick & Luyten, 1996) when  
77 the surf zone is dense relative to surface waters on the shelf, but additional observations  
78 and analyses are needed to understand the dynamics of nearshore plumes.

79 In this paper, airborne infrared and visible observations on the Central California  
80 coast and idealized model simulations with an initially warm or cool surf zone are an-  
81 alyzed to investigate behaviors of plumes generated by rip currents in the presence of  
82 horizontal temperature gradients. In Section 2, observational and modeling methods are  
83 described. Sections 3 and 4 describe and discuss the results, and conclusions are presented  
84 in Section 5.

## 85 2 Methods

### 86 2.1 Airborne observations

87 Airborne remote sensing observations were collected on the Central CA coast near  
88 Point Sal in Sept–Oct 2017 as part of the Office of Naval Research Inner Shelf Depart-  
89 mental Research Initiative. Observations spanned 60-km of coastline with multiple head-  
90 lands, channeled nearshore morphology, and little freshwater influence.

91 Flights with visible and thermal infrared cameras (DRS uc640 microbolometers,  
92 sensitive to 7–14  $\mu\text{m}$ ) were performed on 13 days during daylight hours along several 15-  
93 km segments of coastline. Each 15-km swath, imaging a 2.5 km region from the shore-  
94 line to approximately 20-m depth, was completed in 10 minutes. For the flight altitude  
95 of 3000 ft, the resolution of the visible and infrared imagery is approximately 0.5 m and  
96 2 m, respectively. Two infrared cameras were mounted obliquely and the visible cam-  
97 era was oriented nadir. Images were rectified to geographic coordinates using onboard  
98 GPS and IMU data and intrinsic camera calibrations.

99 Temperature is estimated from the infrared imagery using a linear calibration with  
100 irradiance derived for the sea-surface temperature band, yielding a temperature resolu-  
101 tion of 0.03K (Torgersen et al., 2001; Nugent et al., 2009; Forney et al., 2013). Signals  
102 are predominantly (>90%) emitted at the infrared airborne incidence angles of 20–80°.  
103 The optical depth in water for thermal longwave infrared sensors is 10–20 microns, and  
104 thus the temperature estimates include near-surface ocean temperature variability, in-  
105 cluding the formation and disruption of the millimeter-scale skin-layer, which can be  $O(0.1^\circ\text{C})$   
106 cooler than the bulk water below when there is an outward heat flux from the ocean (Saunders,  
107 1967). In addition, diurnal warm layers  $O(1^\circ\text{C})$  resulting from solar heating lead to tem-  
108 perature stratification in the upper several-meters of the water column (Fairall et al., 1996).  
109 Here, horizontal differences in skin-temperature effects are assumed to be small, and re-  
110 motely sensed temperatures gradients are attributed primarily to differences in near-surface  
111 water-column temperatures.

## 2.2 Idealized modeling of nearshore plumes

Nearshore plumes resulting from bathymetric rip currents are simulated with the Coupled Ocean Wave Atmosphere Sediment Transport modeling system (COAWST), a fully three-dimensional coupled wave-current-sediment transport model that has skill simulating surfzone and inner shelf observations (Warner et al., 2008, 2010; Kumar et al., 2011, 2012, 2015, 2016; Olabarrieta et al., 2014). COAWST couples the ocean circulation model Regional Ocean Modeling System (ROMS) (Haidvogel et al., 2008) with the spectral wave model Simulating WAVes Nearshore (SWAN) (Booij et al., 1996), and includes ocean surface and bottom stresses and surface wave transformation (shoaling, refraction on bathymetry and mean currents, depth-limited breaking, and energy loss due to bottom friction). Processes not included in COAWST, including infragravity variability, short-crested wave breaking, and transient rip currents are expected to drive higher-frequency plume variability that are beyond the focus of this study.

The idealized model domain extends from the shoreline to 23.5-m depth and spans 3 km alongshore with 2-m horizontal resolution and 10 uniformly spaced vertical terrain-following layers (subset of domain shown in Figure 2). The ocean and wave model timestep of 0.5 s and wave-current coupling interval of 15 s were selected for model stability and to resolve timescales of plume evolution. The model is run for 2 hours to simulate the initial plume evolution. The model eddy viscosity is set to  $0.2 \text{ m}^2/\text{s}$ , similar to previous studies (Kumar et al., 2012). To generate bathymetric rip currents that result in nearshore plumes, an idealized wave spectrum similar to nearby observations (JONSWAP spectrum with significant wave height = 1 m, directional spread =  $36^\circ$ , wave period = 7 s,  $\gamma_J = 1.0$ ) is specified at the offshore boundary and waves are incident on a synthetic barred beach profile interrupted by channels (Figure 2). Wave breaking on the channeled bathymetry results in alongshore gradients in wave breaking and setup, driving a bathymetric rip current in each channel (Moulton et al., 2017), with speeds up to 1 m/s. The beach slope (0.025 near shore, concave decreasing slope towards offshore boundary), bar geometry ( $\sim 60$ -m wide,  $\sim 0.5$  m depth at crest), and channel spacing (200 m) and width (40 m) are within the range of observed morphology at the site. Wave and ocean model parameters not described here are the same as used in a previous study of bathymetric rip currents by Moulton et al. (2017).

To simulate a warm or cool surf zone, an initial linear horizontal temperature gradient is applied ( $|\Delta T| = 1^\circ\text{C}$ , as a smooth cross-shore ramp with width  $\sim 30$ -m), with linear vertical stratification on the shelf ( $dT/dz = 0.4^\circ\text{C}/\text{m}$ ) based on observed conditions (Figure 2b,c). A simulation with uniform density also is performed (not shown). Results from simulations with different channel spacing (500 m), initial temperature difference ( $0.5^\circ\text{C}$ ,  $2^\circ\text{C}$ ), and incident wave height (0.5 m and 0.75 m), period (10 s), and spread ( $20^\circ$ ) are qualitatively similar and sensitivity to these parameters is not explored here. In cases run with the same initial temperature distributions and no wave forcing (not shown), plumes do not form, and the horizontal temperature gradients relax slowly. To track water associated with the surfzone-originating plumes, tracer is released continuously near-bed in an alongshore strip in the surf zone (arrows in Figure 2b,c), and is normalized at each time by the total tracer to estimate a fractional tracer concentration, similar to previous studies (Kumar & Feddersen, 2017c; Grimes, Feddersen, & Kumar, 2020).

Model plume lengthscales are normalized by the model surfzone width, defined here as the position where the significant wave height begins decreasing in the region away from channels, here approximately  $L_{sz} \approx 80$  m for 1-m wave height (decreasing to 74 m for 0.75-m waves and 68 m for 0.5-m waves). This location, where depth-limited wave dissipation increases strongly onshore, is expected to be reasonably consistent with the surfzone width identified based on bright foam in visible imagery. The results are not sensitive to the estimate of model surfzone width, which varies by  $O(20\%)$  using other commonly used definitions. Model results are analyzed at several multiples of an approx-

165 imate surfzone flushing timescale, after which the system may have less dependence on  
 166 the surfzone temperature initial condition. For the wave and bathymetric conditions shown  
 167 here, an expected timescale for bathymetric rip currents to flush the surfzone volume is  
 168  $O(15 \text{ min})$ , estimated as the surfzone volume divided by the rip current volume flux per  
 169 unit alongshore width of the domain at the surfzone edge.

### 170 3 Results

#### 171 3.1 Observed plume statistics

172 Signatures of rip-current plumes are ubiquitous in the airborne infrared dataset,  
 173 appearing in the majority of swaths, with  $|\Delta T|$   $0.5\text{--}2^\circ\text{C}$  (Figure 1). The plume loca-  
 174 tions often are fixed in space over hours to days, consistent with bathymetric rip cur-  
 175 rents formed in channels. More transient features with smaller temperature signals and  
 176 shorter spatial scales, possibly resulting from surfzone eddy ejections, also were observed  
 177 but are not studied here. The observed plumes often were cold relative to water on the  
 178 shelf, while warm plumes were observed less frequently, with temperature differences up  
 179 to  $1^\circ\text{C}$  for both cool and warm plumes.

180 Plume presence varied along the complex coastline, possibly as a function of inci-  
 181 dent wave energy and direction, with some sections of coastline experiencing frequent  
 182 strong plume activity, and other regions with few or no observed plumes. A temporal  
 183 pattern was observed during the experiment, with cool plumes more likely to occur in  
 184 the morning, and warm plumes occurring in the afternoon following peak solar heating,  
 185 consistent with previous studies of stochastic eddy ejections (Hally-Rosendahl et al., 2014;  
 186 Grimes, Feddersen, Giddings, & Pawlak, 2020). At some times, both cold and warm plumes  
 187 were present on different parts of the coastline. Changes in plume activity and temper-  
 188 ature with tidal elevation were not evident, however the sensitivity plumes to water lev-  
 189 els and other conditions was not investigated in detail here. On days with large wind speeds  
 190 and wave heights, plumes often were not observed in infrared imagery as a result of weaker  
 191 temperature contrast, however plume signatures were observed under these conditions  
 192 in radar imagery (not shown). During the the selected experiment days analyzed here,  
 193 the tide range was about 1 m, wave heights ranged from 0.5-1.5 m, wave directions were  
 194 primarily from the WNW  $\pm 45^\circ$ , and wind speeds ranged from 1-5 m/s.

195 A subset of the airborne infrared and visible observations were analyzed quanti-  
 196 tatively to identify plume type (warm or cool), surface cross-shore extent (white arrows  
 197 in Figure 1b,c), and surfzone width (arrow in Figure 1a). On the days these quantities  
 198 were estimated, Sept. 16 and Oct. 11, 2017, which were representative of overall exper-  
 199 iment conditions, 97 cool plumes and 92 warm plumes were identified. Manual identi-  
 200 fication of plumes was used for the results shown here after limited success identifying  
 201 plumes using an automated approach using temperature contours. A set of temporally  
 202 and spatially varying surfzone widths selected adjacent to each plume, which varied from  
 203  $L_{sz} = 70\text{--}103\text{m}$  on Sept. 16 and from  $L_{sz} = 96\text{--}145\text{m}$  on Oct. 11, was used for nor-  
 204 malization.

205 Cool and warm plumes both had a wide range of cross-shore extents normalized  
 206 by the surfzone width, with cool plumes having a smaller average cross-shore extent of  
 207  $\langle L_p/L_{sz} \rangle_{cool} = 1.8$  and warm plumes having a larger cross-shore extent of  $\langle L_p/L_{sz} \rangle_{warm} =$   
 208  $2.7$  (Figure 3). The median cool plume extent ( $(L_p/L_{sz})_{med,cool} = 1.7$ ) also differed from  
 209 the median warm plume extent ( $(L_p/L_{sz})_{med,warm} = 2.4$ ) by nearly a surfzone width.  
 210 The peak in the distribution of cool plumes with bins of width 0.5 was  $L_p/L_{sz} \sim 1.5$   
 211 and the distribution is narrower than for warm plumes, which have a broader peak near  
 212  $L_p/L_{sz} \sim 2.0\text{--}2.5$ . The wide distributions of extents (Figure 3) may result partly from  
 213 sampling different stages of the temporal evolution of cool and warm plumes, which formed  
 214 at different times and were observed to change in shape and extent over timescales of

215 tens of minutes to hours. Almost all warm plumes were observed to have cross-shore ex-  
 216 tents of near  $L_p/L_{sz} = 1.5$  or greater, whereas many cool plumes were observed to have  
 217 extent near  $L_p/L_{sz} = 1.0$ . Almost all observed cool plumes had extent less than  $L_p/L_{sz} <$   
 218 4.0, whereas many warm plumes were observed to have  $L_p/L_{sz} > 4.0$  and some warm  
 219 plumes extended as far offshore as  $L_p/L_{sz} \sim 6.0$ .

### 220 3.2 Modeled plumes

221 Idealized model simulations of plumes originating in a cool or warm surf zone and  
 222 extending onto a stratified shelf have similar surface temperature patterns to the remote  
 223 sensing measurements and allow for investigation of subsurface plume behavior (Figure  
 224 1b,c, Figure 4). Initialization of the model with warm or cool surfzone water in other-  
 225 wise identical simulations leads to substantially different cross-shore plume extents and  
 226 vertical structure, suggesting that the relative surf-shelf temperature is a strong control  
 227 on observed plume behavior. Dye in simulations with neutral-density (not shown) and  
 228 the same wave forcing and bathymetry indicates that the surface cross-shore extent of  
 229 neutral-density plumes is typically between that of warm and cool plumes, and that the  
 230 neutral-density plumes show little vertical structure (tracers are well mixed through the  
 231 water column).

232 As modeled rip currents eject surfzone water onto the shelf, the surface temper-  
 233 ature and dye signatures of warm plumes extend further offshore than cool plumes and  
 234 both have complex patterns. Similar to field observations (Figure 1b,c), the alongshore  
 235 surface structure of cool and warm plumes differed significantly, with warm plumes ex-  
 236 hibiting more lateral spreading and more rounded patterns, and cool plumes having nar-  
 237 rower alongshore scales and more complex structure at the plume edges (Figure 4a,b).  
 238 Both warm and cool plumes contain filaments of cooler or warmer water. At time  $t=45$   
 239 min, the cross-shore extent of modeled cool plumes is approximately  $(L_p/L_{sz})_{cool} \approx 1.8-$   
 240 3, whereas for warm plumes  $(L_p/L_{sz})_{cool} \approx 3.8-4$  (Figure 4a,b). The modeled warm  
 241 plumes extend approximately one surfzone width farther offshore at this time, similar  
 242 to bulk results from field observations sampling temporally complex plume evolution (Fig-  
 243 ure 3).

244 To simulate variability in temporal sampling and conditions similar to the field sam-  
 245 pling, four additional simulations were analyzed for both cool and warm plumes, two with  
 246 different initial  $|\Delta T|$  ( $0.5^\circ\text{C}$ ,  $2^\circ\text{C}$ ) and two with different incident wave heights (0.5 m  
 247 and 0.75 m), resulting in a suite of five simulations each for cool and warm plumes. Each  
 248 of these simulations was analyzed for plume cross-shore extent near the five channel lo-  
 249 cations at four randomly selected times (using model output at 5-min intervals from 5-  
 250 60 min), yielding estimates for 100 cool plumes and 100 warm plumes. Results are not  
 251 sensitive to removing half of the randomly sampled times. The resulting distributions  
 252 of cool and warm plume surface extents (Figure 4c,d) had average extents of  $\langle L_p/L_{sz} \rangle_{cool} =$   
 253 2.4 and  $\langle L_p/L_{sz} \rangle_{warm} = 3.6$ ; warm plumes extended on average approximately one sur-  
 254 fzone width further offshore than cool plumes, similar to the observations (Figure 3). Me-  
 255 dian plume extents are similar to the average extents. The modeled distributions have  
 256 larger mean and median values than the observations, which may result from different  
 257 sampling of conditions and times. Like the observations, cool plumes had a narrower dis-  
 258 tribution of cross-shore surface extents, whereas warm plumes had a wider distribution  
 259 with more plumes observed at large cross-shore extents.

260 To investigate plume vertical structure, temperature and dye transects are shown  
 261 in Figure 4e-j. The dye and temperature fields were averaged over 40-m (the channel width)  
 262 centered at  $y=200$  m (the center of one of the channels). In modeled cool plumes, surfzone-  
 263 released tracer subducts to a level of neutral density into the stratified shelf (Figure 4e,f,g),  
 264 similar to modeled behavior of transient rip currents (Kumar & Feddersen, 2017a; Grimes,  
 265 Feddersen, & Kumar, 2020). In warm plumes, buoyant surfzone water is confined to the

266 surface, enhancing near-surface stratification (Figure 4h,i,j). Cool or warm water leaves  
 267 the surf zone in a momentum-dominated jet, and subsequently lifts off and propagates  
 268 slowly offshore, consistent with the transition from a jet to a gravity current. The plume  
 269 liftoff location, approximately where temperature contours intersect the bed, is consis-  
 270 tent at each time with the location where a baroclinic Froude number reaches unity (Fig-  
 271 ure 4e-j, triangles). Here this Froude number is defined for nearshore plumes as  $Fr_p =$   
 272  $U_p/\sqrt{g'h}$ , where  $U_p$  is the depth-averaged plume velocity and  $\sqrt{g'h}$  is a baroclinic phase  
 273 speed, a function of the reduced gravity  $g'$  (here set as a constant value set by  $\Delta T =$   
 274  $1^\circ\text{C}$ ) and the water depth  $h$ . The plume velocity  $U_p$  and the water depth  $h$  both vary  
 275 in the cross-shore, and are estimated as averages over 40-m alongshore distance.

276 At later times in the simulation (not shown), the warm water initialized in the surf  
 277 zone flushes out and the ejected warm water continues to laterally spread and mix, with  
 278 a decaying plume temperature signature. In contrast, cool plumes continue to persist be-  
 279 yond several surfzone flushing timescales, possibly as a result of continued entrainment  
 280 of cool water into the surf zone. The persistent cool plumes have a relatively fixed cross-  
 281 shore extent at the surface, the location where cool water subducts, and an increasing  
 282 subsurface dye extent as the cool gravity current continues to propagate offshore.

## 283 4 Discussion

284 The observed spatial gradients in temperature between the surf zone and inner shelf  
 285 may occur as a result of variations in water depth, solar heating, wave dissipation, and  
 286 other processes. If both the shelf and surf zone are well mixed, the shallower surf zone  
 287 may heat and cool more quickly in the presence of a spatially uniform diurnally vary-  
 288 ing surface heat flux, contributing to the observed occurrence of warm plumes follow-  
 289 ing periods of strong heating. This spatial gradient in diurnal heating also leads to a di-  
 290 urnally reversing horizontal temperature gradient (Ulloa et al., 2018) driving a net two-  
 291 layer cross-shore circulation that is expected to be small relative to rip-current-driven  
 292 transport (Grimes, Feddersen, & Kumar, 2020). In contrast, under weak mixing condi-  
 293 tions (e.g., low winds), a diurnal warm layer (Price et al., 1986) may form on the shelf,  
 294 leading to warmer near-surface temperatures offshore of the surf zone during strong solar  
 295 heating.

296 Other contributors to horizontal temperature gradients include spatial variations  
 297 in albedo resulting from bright wave-breaking-generated foam (Sinnott & Feddersen, 2014),  
 298 elevated turbidity from suspended sediment or algae (Fogarty et al., 2018), transfer of  
 299 heat stored in the sediments of the intertidal beach (Rinehimer & Thomson, 2014), and  
 300 heating due to wave dissipation (Sinnott & Feddersen, 2014). In addition, wind-driven  
 301 flows, regional coastal circulation patterns, and propagating fronts and internal waves  
 302 may drive or modulate horizontal density gradients in this region (Washburn et al., 2011;  
 303 Sinnott et al., 2018; McSweeney et al., 2020; Feddersen et al., 2020). Prior results sug-  
 304 gest these processes may drive the observed horizontal surface temperature gradients of  
 305  $O(1^\circ\text{C})$  with variability on diurnal, synoptic, and seasonal timescales, however, the tem-  
 306 poral variation and relative importance of these processes is not known. In addition, the  
 307 nearshore plume behavior may vary as a result of interaction with shelf processes includ-  
 308 ing internal waves, fronts, and adjacent plumes.

309 Horizontal differences in near-surface mixing and resulting disruption of cool skins  
 310 or diurnal warm layers (Saunders, 1967; Fairall et al., 1996) may contribute to the ob-  
 311 served temperature differences between the surf zone and the shelf. The results here are  
 312 not expected to be affected by  $O(0.1^\circ\text{C})$  differences in cool-skin formation that may oc-  
 313 cur as a result of differences in near-surface mixing between the surf zone and the shelf.  
 314 Diurnal warm layer formation  $O(1^\circ\text{C})$  enhances near-surface stratification and may af-  
 315 fect interpretation of the remote sensing measurements and the vertical structure of plumes.  
 316 Future work incorporating models of the upper ocean temperature profile behavior (Fairall

317 et al., 2003) is needed to use the airborne measurements to infer subsurface tempera-  
 318 ture gradients with higher accuracy.

319 Results shown here indicate commonalities between nearshore plumes generated  
 320 by rip currents and small buoyant plumes or subducting gravity currents. Still, further  
 321 study is needed to improve understanding of these features, including controls on mix-  
 322 ing and entrainment at plume boundaries, rates of plume spreading, cross-shore exchange,  
 323 and the temporal evolution of plumes at timescales from individual waves to diurnal to  
 324 seasonal forcing. Further comparison of uniform and variable-density plume behavior will  
 325 aid understanding of how rip-current vertical structure is modulated by density. While  
 326 this analysis focused on temperature variability, the results may be applicable to salin-  
 327 ity variations near small river mouths where freshwater transported along-coast escapes  
 328 through the surf zone. The airborne images and model initial-condition experiments pre-  
 329 sented here provide insight into bulk differences between warm and cool nearshore plumes  
 330 driven by rip currents.

## 331 5 Conclusions

332 Airborne infrared imagery on the California coast shows cool and warm plumes con-  
 333 necting the surf zone to the inner shelf. These plumes are driven by rip currents in the  
 334 surf zone that transport water offshore in a narrow jet that transitions to a buoyancy-  
 335 controlled plume. In both observations and simulations, the surface cross-shore extent  
 336 of warm plumes is about one surfzone width larger than that of cool plumes. Modeled  
 337 cool nearshore plumes entering a stratified shelf subduct to a level of neutral density, whereas  
 338 warm plumes extend offshore in a near-surface layer. This work indicates that the tem-  
 339 perature of rip-current plumes affects the horizontal and vertical structure of the exchange  
 340 of tracers from the surf zone to the shelf.

## 341 Acknowledgments

342 Observations were collected as part of the Office of Naval Research Inner Shelf Dynam-  
 343 ics Experiment effort to study inner shelf processes. Additional support was provided  
 344 by the University of Washington Royalty Research Fund and the Office of Naval Research  
 345 Young Investigator Program. Thanks to experiment participants for a team effort to col-  
 346 lect field measurements and for providing feedback on this work. Observations are avail-  
 347 able in the Inner Shelf data repository hosted by UC San Diego Library (<https://doi.org/10.6075/J0WD3Z3Q>)  
 348 and model results and input files are available at Zenodo.org (<https://doi.org/10.5281/zenodo.4272080>).

## 349 References

- 350 Boehm, A. B., Ismail, N. S., Sassoubre, L. M., & Andruszkiewicz, E. A. (2017).  
 351 Oceans in Peril: Grand Challenges in Applied Water Quality Research for  
 352 the 21st Century. *Environmental Engineering Science*, *34*(1), 3–15. doi:  
 353 10.1089/ees.2015.0252
- 354 Booij, N., Holthuijsen, L. H., & Ris, R. C. (1996). The "SWAN" Wave Model for  
 355 Shallow Water. *Coastal Engineering*, 668–676. doi: 10.9753/icce.v25.p
- 356 Bowen, A. J. (1969). Rip currents: 1. Theoretical investigations. *Journal of Geo-*  
 357 *physical Research*, *74*(23), 5467. doi: 10.1029/JC074i023p05467
- 358 Castelle, B., Scott, T., Brander, R., & McCarroll, R. (2016). Rip Current Types,  
 359 Circulation and Hazard. *Earth-Science Reviews*, *163*, 1–21. doi: 10.1016/j  
 360 .earscirev.2016.09.008
- 361 Cole, K. L., & Hetland, R. D. (2016). The effects of rotation and river discharge  
 362 on net mixing in small mouth Kelvin number plumes. *Journal of Physical*  
 363 *Oceanography*, *46*(2010), 1421–1436. doi: 10.1175/JPO-D-13-0271.1
- 364 Dalrymple, R. a., MacMahan, J. H., Reniers, A. J. H. M., & Nelko, V. (2011, jan).

- 365 Rip Currents. *Annual Review of Fluid Mechanics*, 43(1), 551–581. doi: 10  
 366 .1146/annurev-fluid-122109-160733
- 367 Fairall, C. W., Bradley, E. F., Godfrey, J. S., Wick, G. A., Edson, J. B., & Young,  
 368 G. S. (1996). Cool-skin and warm-layer effects on sea surface tempera-  
 369 ture. *Journal of Geophysical Research: Oceans*, 101(C1), 1295–1308. doi:  
 370 10.1029/95JC03190
- 371 Fairall, C. W., Bradley, E. F., Hare, J. E., Grachev, A. A., & Edson, J. B.  
 372 (2003). Bulk parameterization of air-sea fluxes: Updates and verifica-  
 373 tion for the COARE algorithm. *Journal of Climate*, 16(4), 571–591. doi:  
 374 10.1175/1520-0442(2003)016<0571:BPOASF>2.0.CO;2
- 375 Feddersen, F., MacMahan, J. H., Freismuth, T. M., Gough, M. K., & Kovatch, M.  
 376 (2020). Inner-Shelf Vertical and Alongshore temperature Variability in the  
 377 Subtidal, Diurnal, and Semidiurnal Bands Along the central California coast-  
 378 line with headlands. *Journal of Geophysical Research: Oceans*, 125(3), 1–24.  
 379 doi: 10.1029/2019jc015347
- 380 Fogarty, M. C., Fewings, M. R., Paget, A. C., & Dierssen, H. M. (2018). The Influ-  
 381 ence of a Sandy Substrate, Seagrass, or Highly Turbid Water on Albedo and  
 382 Surface Heat Flux. *Journal of Geophysical Research: Oceans*, 123, 53–73. doi:  
 383 10.1002/2017JC013378
- 384 Forney, W. M., Souldard, C. E., & Chickadel, C. C. (2013). Salmonids, Stream  
 385 Temperatures, and Solar Loading—Modeling the Shade Provided to the Kla-  
 386 math River by Vegetation and Geomorphology. *USGS Scientific Investigations*  
 387 *Report 2013-5022*.
- 388 Grant, S. B., Kim, J. H., Jones, B. H., Jenkins, S. A., Wasyl, J., & Cudaback, C.  
 389 (2005). Surf zone entrainment, along-shore transport, and human health im-  
 390 plications of pollution from tidal outlets. *Journal of Geophysical Research C:*  
 391 *Oceans*, 110(10), 1–20. doi: 10.1029/2004JC002401
- 392 Grimes, D. J., Feddersen, F., Giddings, S. N., & Pawlak, G. (2020). Cross-  
 393 shore deformation of a surfzone released dye plume by an internal tide on  
 394 the inner-shelf. *Journal of Physical Oceanography*, 50(1), 35–54. doi:  
 395 10.1175/JPO-D-19-0046.1
- 396 Grimes, D. J., Feddersen, F., & Kumar, N. (2020). Tracer Exchange Across  
 397 the Stratified Inner-Shelf Driven by Transient Rip-Currents and Diurnal  
 398 Surface Heat Fluxes. *Geophysical Research Letters*, 47(10), 1–12. doi:  
 399 10.1029/2019GL086501
- 400 Haidvogel, D. B., Arango, H., Budgell, W. P., Cornuelle, B. D., Curchitser, E., Di  
 401 Lorenzo, E., . . . Wilkin, J. L. (2008). Ocean forecasting in terrain-following  
 402 coordinates: Formulation and skill assessment of the Regional Ocean Mod-  
 403 eling System. *Journal of Computational Physics*, 227(7), 3595–3624. doi:  
 404 10.1016/j.jcp.2007.06.016
- 405 Haller, M. C., Honegger, D. A., & Catalán, P. (2014). Rip current observations  
 406 via marine radar. *Journal of Waterway, Port, Coastal, and Ocean Engineer-*  
 407 *ing*, 140(April), 115–124. doi: 10.1061/(ASCE)WW.1943-5460.0000229.
- 408 Hally-Rosendahl, K., Feddersen, F., & Guza, R. T. (2014). Cross-shore tracer ex-  
 409 change between the surfzone and inner-shelf. *Journal of Geophysical Research:*  
 410 *Oceans*, 119(7), 4367–4388. doi: 10.1002/2013JC009722
- 411 Kastner, S. E., Horner-Devine, A. R., & Thomson, J. M. (2019). A Conceptual  
 412 Model of a River Plume in the Surf Zone. *Journal of Geophysical Research:*  
 413 *Oceans*, 124(11), 8060–8078. doi: 10.1029/2019JC015510
- 414 Kumar, N., & Feddersen, F. (2017a). The Effect of Stokes Drift and Transient Rip  
 415 Currents on the Inner Shelf. Part II: With Stratification. *Journal of Physical*  
 416 *Oceanography*, 47(1), 243–260. doi: 10.1175/JPO-D-16-0077.1
- 417 Kumar, N., & Feddersen, F. (2017b). The Effect of Stokes Drift and Transient  
 418 Rip Currents on the Inner Shelf. Part I: No Stratification. *Journal of Physical*  
 419 *Oceanography*, 47(1), 227–241. doi: 10.1175/JPO-D-16-0076.1

- 420 Kumar, N., & Feddersen, F. (2017c). A new offshore transport mechanism for  
 421 shoreline-released tracer induced by transient rip currents and stratification.  
 422 *Geophysical Research Letters*, *44*(6), 2843–2851. doi: 10.1002/2017GL072611
- 423 Kumar, N., Feddersen, F., Suanda, S., Uchiyama, Y., & McWilliams, J. (2016). Mid-  
 424 to Inner-Shelf Coupled ROMS–SWAN Model–Data Comparison of Currents  
 425 and Temperature: Diurnal and Semidiurnal Variability. *Journal of Physical*  
 426 *Oceanography*, *46*(3), 841–862. doi: 10.1175/JPO-D-15-0103.1
- 427 Kumar, N., Feddersen, F., Uchiyama, Y., McWilliams, J. C., & O’Reilly, W.  
 428 (2015). Midshelf to Surfzone Coupled ROMS–SWAN Model Data Compar-  
 429 ison of Waves, Currents, and Temperature: Diagnosis of Subtidal Forcings  
 430 and Response. *Journal of Physical Oceanography*, *45*(6), 1464–1490. doi:  
 431 10.1175/JPO-D-14-0151.1
- 432 Kumar, N., Voulgaris, G., & Warner, J. C. (2011, dec). Implementation and mod-  
 433 ification of a three-dimensional radiation stress formulation for surf zone  
 434 and rip-current applications. *Coastal Engineering*, *58*(12), 1097–1117. doi:  
 435 10.1016/j.coastaleng.2011.06.009
- 436 Kumar, N., Voulgaris, G., Warner, J. C., & Olabarrieta, M. (2012). Implementation  
 437 of the vortex force formalism in the coupled ocean-atmosphere-wave-sediment  
 438 transport (COAWST) modeling system for inner shelf and surf zone applica-  
 439 tions. *Ocean Modelling*, *47*, 65–95. doi: 10.1016/j.ocemod.2012.01.003
- 440 Marmorino, G. O., Smith, G. B., & Miller, W. D. (2013). Infrared remote sens-  
 441 ing of surf-zone eddies. *IEEE Journal of Selected Topics in Applied Earth Ob-*  
 442 *servations and Remote Sensing*, *6*(3), 1710–1718. doi: 10.1109/JSTARS.2013  
 443 .2257695
- 444 McSweeney, J. M., Lerczak, J. A., Barth, J. A., Becherer, J., Colosi, J. A., Mackin-  
 445 non, J. A., . . . Waterhouse, A. F. (2020). Observations of shoaling nonlinear  
 446 internal bores across the Central California inner shelf. *Journal of Physical*  
 447 *Oceanography*, *50*(1), 111–132. doi: 10.1175/JPO-D-19-0125.1
- 448 Morgan, S. G., Shanks, A. L., MacMahan, J. H., Reniers, A. J., & Feddersen,  
 449 F. (2018). Planktonic subsidies to surf-zone and intertidal communi-  
 450 ties. *Annual Review of Marine Science*, *10*, 345–369. doi: 10.1146/  
 451 annurev-marine-010816-060514
- 452 Moulton, M., Elgar, S., Raubenheimer, B., Warner, J. C., & Kumar, N. (2017).  
 453 Rip currents and alongshore flows in single channels dredged in the surf  
 454 zone. *Journal of Geophysical Research: Oceans*, *122*(5), 3799–3816. doi:  
 455 10.1002/2016JC012222
- 456 Nugent, P. W., Shaw, J. A., Pust, N. J., & Piazzolla, S. (2009). Correcting cal-  
 457 ibrated infrared sky imagery for the effect of an infrared window. *Jour-*  
 458 *nal of Atmospheric and Oceanic Technology*, *26*(11), 2403–2412. doi:  
 459 10.1175/2009JTECHA1288.1
- 460 Olabarrieta, M., Geyer, W. R., & Kumar, N. (2014). The role of morphology  
 461 and wave-current interaction at tidal inlets: An idealized modeling analy-  
 462 sis. *Journal of Geophysical Research: Oceans*, *119*(12), 8818–8837. doi:  
 463 10.1002/2014JC010191
- 464 Price, J. F., Weller, R. A., & Pinkel, R. (1986). Diurnal Cycling: observations  
 465 and models of the upper ocean response to diurnal heating, cooling, and wind  
 466 mixing. *Journal of Geophysical Research: Oceans*, *91*(6), 8411–8427. doi:  
 467 10.1029/jc091ic07p08411
- 468 Rinehimer, J. P., & Thomson, J. T. (2014). Observations and modeling of heat  
 469 fluxes on tidal flats. *Journal of Geophysical Research: Oceans*, *119*(1), 133–  
 470 146. doi: 10.1002/2013JC009225
- 471 Rudnick, D. L., & Luyten, J. R. (1996). Intensive surveys of the Azores Front 1.  
 472 Tracers and dynamics. *Journal of Geophysical Research C: Oceans*, *101*(C1),  
 473 923–939. doi: 10.1029/95JC02867
- 474 Saunders, P. M. (1967). The Temperature at the Ocean–Air Interface. *Journal of the*

- 475 *Atmospheric Sciences*, 24(3), 269–273. doi: 10.1175/1520-0469(1967)024<0269:  
476 ttatoa>2.0.co;2
- 477 Sinnett, G., & Feddersen, F. (2014). The surf zone heat budget: The effect  
478 of wave heating. *Geophysical Research Letters*, 41(20), 7217–7226. doi:  
479 10.1002/2014GL061398
- 480 Sinnett, G., Feddersen, F., Lucas, A. J., Pawlak, G., & Terrill, E. (2018). Observa-  
481 tions of Nonlinear Internal Wave Run-Up to the Surfzone. *Journal of Physical  
482 Oceanography*, 48(3), 531–554. doi: 10.1175/JPO-D-17-0210.1
- 483 Smith, J. A., & Largier, J. L. (1995). Observations of nearshore circulation: Rip  
484 currents. *Journal of Geophysical Research*, 100(C6), 10967. doi: 10.1029/  
485 95JC00751
- 486 Suanda, S. H., & Feddersen, F. (2015). A self-similar scaling for cross-shelf exchange  
487 driven by transient rip currents. *Geophysical Research Letters*, 42(13), 5427–  
488 5434. doi: 10.1002/2015GL063944
- 489 Torgersen, C. E., Faux, R. N., McIntosh, B. A., Poage, N. J., & Norton, D. J.  
490 (2001). Airborne thermal remote sensing for water temperature assessment  
491 in rivers and streams. *Remote Sensing of Environment*, 76(3), 386–398. doi:  
492 10.1016/S0034-4257(01)00186-9
- 493 Ulloa, H. N., Davis, K. A., Monismith, S. G., & Pawlak, G. (2018). Temporal  
494 variability in thermally driven cross-shore exchange: The role of semidi-  
495 urnal tides. *Journal of Physical Oceanography*, 48(7), 1513–1531. doi:  
496 10.1175/JPO-D-17-0257.1
- 497 Warner, J. C., Armstrong, B., He, R., & Zambon, J. B. (2010, jan). Development of  
498 a Coupled Ocean-Atmosphere-Wave-Sediment Transport (COAWST) Modeling  
499 System. *Ocean Modelling*, 35(3), 230–244. doi: 10.1016/j.ocemod.2010.07.010
- 500 Warner, J. C., Butman, B., & Dalyander, P. S. (2008). Storm-driven sediment trans-  
501 port in Massachusetts Bay. *Continental Shelf Research*, 28(2), 257–282. doi:  
502 10.1016/j.csr.2007.08.008
- 503 Washburn, L., Fewings, M. R., Melton, C., & Gotschalk, C. (2011). The propagating  
504 response of coastal circulation due to wind relaxations along the central Cal-  
505 ifornia coast. *Journal of Geophysical Research: Oceans*, 116(12), 1–16. doi:  
506 10.1029/2011JC007502

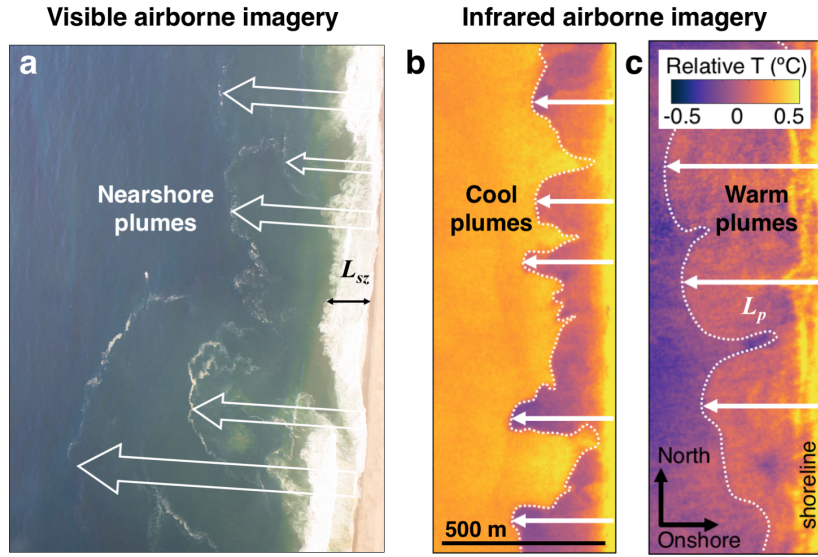


**Figure 1.** (a) Aerial photo of the surf zone and inner shelf along several km of coast near Pt. Sal, CA, with nearshore plumes generated by rip currents carrying sediment offshore (arrows). Airborne infrared images (georectified, scale in b) showing relative temperature ( $^{\circ}\text{C}$ ), with (b) cool and (c) warm plumes (dashed temperature contours: plume boundaries; arrows: plume cross-shore extent  $L_p$ ) originating in the surf zone (width  $L_{sz}$  in a) and extending 100s of m onto the shelf.

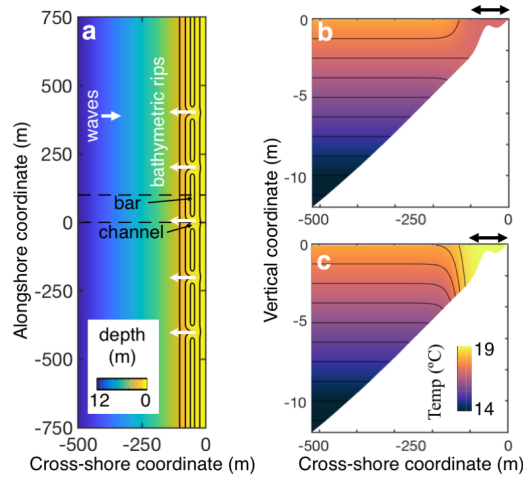


**Figure 2.** (a) Idealized COAWST model domain (subset of domain shown) with barred bathymetry (color contours) interrupted by a series of channels, and initial cross-shore temperature sections (color, with contours every  $0.5^{\circ}\text{C}$ ) for (b) cool surf zone (c) warm surf zone ( $|\Delta T|=1^{\circ}\text{C}$ ) with linear shelf stratification. Wave breaking on the bar-channel bathymetry drives a series of bathymetric rip-current jets (a, white arrows) that emerge on the shelf as nearshore plumes, tracked here with passive tracer released in the surf zone (b,c black arrows).

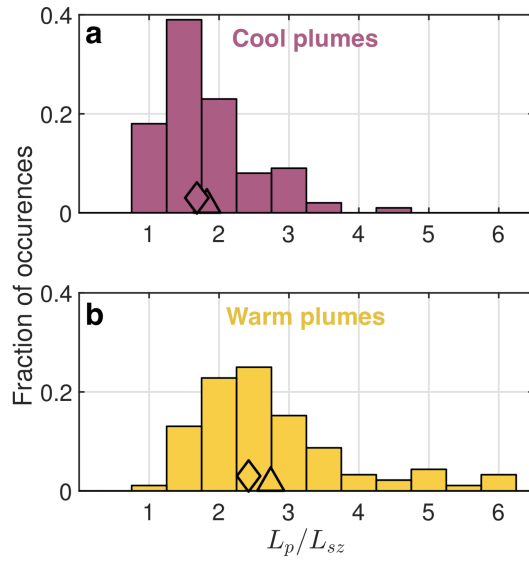


**Figure 3.** Histograms of the number of occurrences of (a) cool and (b) warm plumes in infrared imagery versus the ratio of the plume cross-shore surface extent ( $L_p$ , arrows in Fig. 1b,c) and surfzone width ( $L_{sz}$ , Fig. 1a). The average cross-shore surface extent (triangle on x axis) is  $\langle L_p/L_{sz} \rangle_{cool} = 1.8$  for cool plumes and  $\langle L_p/L_{sz} \rangle_{warm} = 2.7$  for warm plumes, and the median cross-shore surface extent (diamond on x axis) is  $(L_p/L_{sz})_{med,cool} = 1.7$  for cool plumes and  $(L_p/L_{sz})_{med,warm} = 2.4$  for warm plumes.

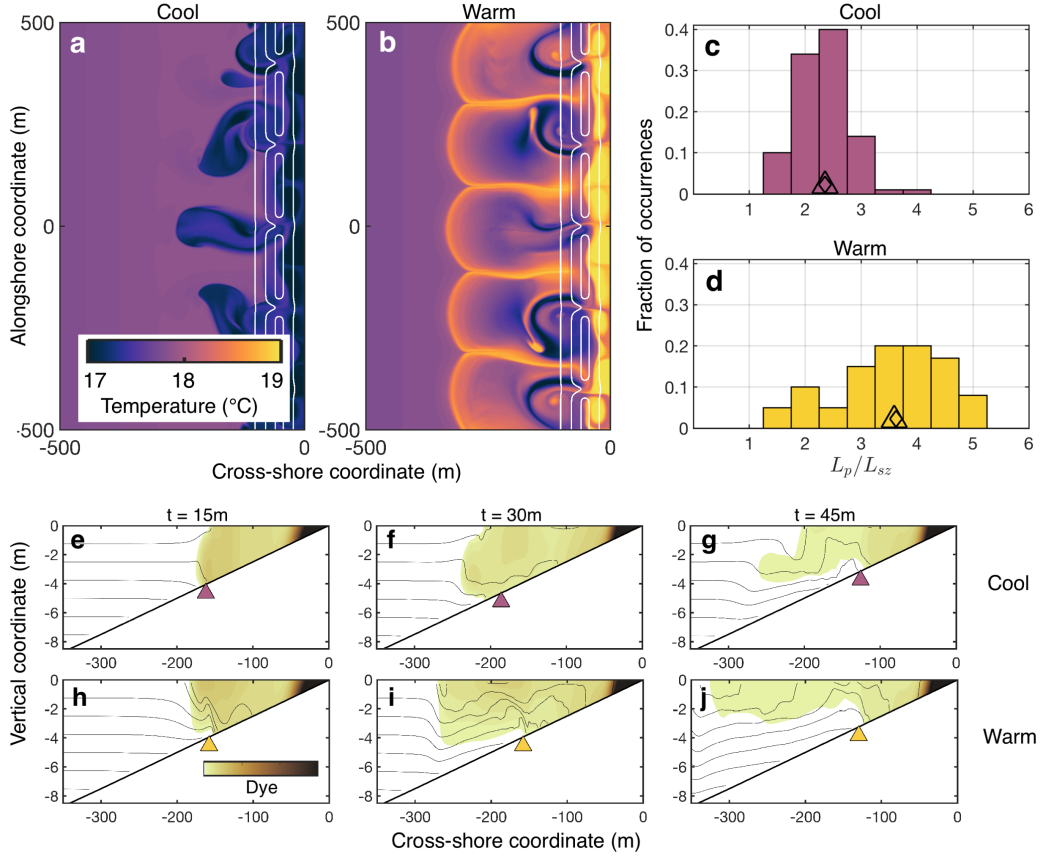


**Figure 4.** Surface temperature for modeled (a) cool and (b) warm plumes with initial temperature difference between the surf zone and the shelf of  $|\Delta T| = 1^\circ\text{C}$  (Figure 2) at  $t=45$  mins. Histograms of the fractional number of occurrences of (c) cool and (d) warm plumes in a suite of model simulations sampled at a range of times versus the normalized plume cross-shore extent (triangle: average, diamond: median). Cross-shore vertical sections of temperature (contours every  $0.5^\circ\text{C}$ ) and the relative concentration of surfzone-released dye (color) through the center of a plume ( $y=200$  m) for (e, f, g) cool or (h, i, j) warm plumes at  $t=15$  min (e, h),  $t=30$  min (f, i), and  $t=45$  min (g, j). Triangles in (e-j) are locations where a baroclinic plume Froude number reaches unity, which approximately predicts plume liftoff.